SIMULATION OF DISTRIBUTIVE AND DISPERSIVE MIXING IN A CO-ROTATING TWIN-SCREW EXTRUDER

L. Cong and M. Gupta
Michigan Technological University, Houghton, MI, 49931

Abstract

Simulation results for mixing of two different polymers in a co-rotating twin-screw extruder are presented. Velocity distribution predicted by a three-dimensional simulation of the flow is used to predict the change in the spatial distribution of initially segregated particles as well as the reduction in radius due to erosion. The predicted particle distribution is used to estimate the increase in Shannon entropy due to dispersive and distributive mixing along the extruder channel.

Introduction

Dispersive mixing refers to the break-up of the minor component of a mixture into smaller size particles or droplets, whereas distributive mixing leads to a homogeneous spatial distribution of the minor component into the polymer matrix [1]. A three-dimensional simulation of the flow can be exploited as an excellent aide for analysis of dispersive as well as distributive mixing in screw extruders. The predicted velocity distribution along with a particle tracing scheme for finding path lines can be employed to predict the mixing efficiency in screw extruders. In references [1, 2], this methodology was applied to study the mixing in single-screw extruders. Implementation of a particle tracing algorithm for a single-screw extruder is relatively simple because a time-independent flow field can be obtained by keeping the screw stationary and rotating the barrel in the direction opposite to the screw rotation direction. In comparison to single-screw extruders, the flow in twin-screw extruders is much more complicated. Besides the increased complexity of geometry, the time-dependent flow in a twin-screw extruder cannot be transformed into a steady state flow by fixing the coordinate frame on a screw. Because of the time-dependent nature of the flow, the predicted velocity distribution for a single configuration of the two screws cannot be used to trace the path lines in a twin-screw extruder. However, in a reference frame moving with axial velocity $V_{ref} = LN$ towards the exit, where L is the screw lead and N is the rotational speed in revolution per second, the flow field in a twin-screw extruder is time independent. In the present work, a particle tracing scheme was developed to trace path lines in this translating reference frame. Quality of distributive mixing in a co-rotating twin-screw extruder was evaluated by finding the change in the spatial distribution of initially segregated particles. For the same twin-screw extruder, quality of dispersive mixing was

determined by using the erosion model of Manas-Zloczower *et al.* [1, 2].

Shannon Entropy of a Mixture

Following the approach of Manas-Zloczower and co-workers [1], in the present work Shannon entropy [3] is used as a measure of the quality of mixing. For mixing of two different types of particles (red and blue), if the flow domain at each cross section is divided into *M* equal-sized bins, Shannon entropy (*S*) in defined as

$$S = -\sum_{c=1}^{2}\sum_{j=1}^{M} P_{c,j} \ln P_{c,j} \qquad (1)$$

where *c* represents the particle type (red or blue) and $P_{c,j}$ is the probability of finding particle of color *c* in bin *j*.

To estimate the homogeneity of color, Manas-Zloczower *et al.* [1] subtracted the entropy associated with the overall spatial distribution of particles (irrespective of the type of particles) ($-\sum_{j=1}^{M} P_j \ln P_j$) from the Shannon entropy, resulting in a quantity called color homogeneity index (CHI).

$$\text{CHI} = (S + \sum_{j=1}^{M} P_j \ln P_j)/\ln(2) \qquad (2)$$

where P_j is the probability of finding a particle (irrespective of color) in bin and the division by ln(2) is used to normalize the index such that its value lies between 0 and 1.

Erosion Model for Porous Agglomerate

Two different types of mechanisms, namely, rupture and erosion, are often employed to analyze dispersive mixing. Rupture refers to break-up of a particle or drop into two parts of comparable size. For erosion, the original particle or drop is modeled as an agglomerate of smaller particles or droplets, which are detached or 'peeled' off the agglomerate surface. The erosion model developed by Scurati *et al.* [4, 5] is employed in the present work to predict the quality of dispersive mixing. Scurati *et al.* [4, 5] postulated that reduction in radius (*R*) of an agglomerate in a shear flow is proportional to the shear rate ($\dot{\gamma}$) and the difference between the hydrodynamic (F_h) and cohesive (F_c) forces.

$$-\frac{dR}{dt} = K(F_h - F_c)\frac{\dot{\gamma}}{2} \qquad (4)$$

where *K* is the proportional coefficient. Scurati *et al.* [4, 5] assumed that during erosion the agglomerate maintains a

spherical shape. Furthermore, it was assumed in references [4, 5] that a fragment is removed from the agglomerate only when reduction in radius of the agglomerate is equal to a predetermined volume of the fragment and the fragment is also assumed to have a spherical shape. The fragment is assumed to be the smallest size particle in the system, and therefore does not erode any further. Also, once the size of an agglomerate is reduced to that of a fragment, the erosion of the agglomerate is stopped. In order to estimate the cohesive force (F_c), Scurati *et al.* [4, 5] modeled the polymer agglomerate as a fragmented fractal porous medium with non-uniform porosity, given by the following equation $\rho/\rho_0 = (R/R_0)^{D-3}$, where ρ and ρ_0 are densities of agglomerate at radius R and initial radius R_0 respectively and D, called the fractal dimension, is 3 for an agglomerate with zero porosity and less than 3 for a porous agglomerate. It can be shown [4, 5] that the cohesive force between the fragmental cap shown in Fig. 1 and the remaining fractal porous agglomerate is given by

$$F_c = \pi\sigma_0 \frac{2}{D-1} \frac{R^{D-1}}{R_0^{D-3}} \left(1 - \cos^{D-1}\psi_0\right) \qquad (5)$$

where σ_0 is the characteristic cohesive force per unit area and ψ_0, shown in Fig. 1, specifies the size of the fragmental cap.

Assuming that erosion of fractal porous agglomerate is mainly caused by the normal component of hydrodynamic force on the agglomerate [4, 5], the following equation gives an estimate for the hydrodynamic force (F_h) in a simple shear flow

$$F_h = F_N = \frac{5}{2}\mu\pi\dot{\gamma}R^2 \sin^2\psi_0 \cos^2\phi \sin 2\theta \qquad (6)$$

where the angles θ and ϕ in Fig. 1 specify the unit vector along the line connecting the center of the spherical agglomerate to the center of the circular area of the fragmental cap.

Since elongational flows are known to result in higher dispersive mixing [6], Wang *et al.* [7, 8] used an ad hoc modification of Eqn. (6) which gives larger hydrodynamic force for elongational flow.

$$F_h = 5\lambda\mu\pi\dot{\gamma}R^2 \sin^2\psi_0 \cos^2\phi \sin 2\theta \qquad (7)$$

where λ, called flow strength, is defined as $\lambda = \dot{\gamma}/(\dot{\gamma}+\omega)$ with ω being the norm of vorticity tensor. The flow strength is 1 for elongational flow, 1/2 for simple shear flow and 0 for rotational flow. Substitution of Eqn. (5) and (7) into Eqn. (4) gives the equation for erosion of a fractal porous agglomerate. For the simulation presented later in this paper, the values of K, D, σ_0 and ψ_0 employed are 0.0005, 2.7, 1000 Pa, and $10°$ respectively.

Particle Tracing Scheme with Rotating Screw

As discussed previously, calculation of the color homogeneity index in the extruder is based upon the change in the spatial distribution of different color particles, which are placed in a segregated configuration at the entrance. The change in the spatial distribution of the particle can be determined by following their path lines to the desired axial location of the extruder. For a steady, time-independent flow, path lines can be easily determined by updating the location of the particle in each time step (Δt) by the following equation.

$$\vec{X}(t + \Delta t) = \vec{X}(t) + \vec{v}(t)\Delta t \qquad (8)$$

where $\vec{X}(t)$ and $\vec{X}(t + \Delta t)$ are the positions of particle at the current time t and at time $t + \Delta t$ respectively, and $\vec{v}(t)$ is the velocity at the current location $\vec{X}(t)$. However, such a scheme cannot be extended beyond one time step for time-dependent flows such as the flow in an extruder with rotating screw. For instance, for point A in Fig. 2 (a), the position of A' after time step Δt, can be determined using Eqn. (8). However, to extend the path line of particle A beyond $t + \Delta t$, the velocity at point A' is required in the screw configuration at time $t + \Delta t$, and not the velocity at A' in the configuration at time t. The velocity at point A' in the screw configuration at time $t + \Delta t$ can be determined from the velocity distribution in the screw configuration at time t if the translational reference frame mentioned earlier is employed for the calculation. As mentioned before, in a reference frame moving along the axial direction with velocity V_{ref} as described above the geometry of a screw extruder is time independent. The time-independent nature of a screw extruder flow domain in this moving reference frame is clear from Fig. 2 (b), which shows the configuration of the screw in Fig. 2 (a) after $t = 1/(2N)$, that is, after one half screw rotation. In the moving reference frame, point B at time t in Fig. 1 (a) is mapped to point B' at time $t' = t + 1/(2N)$ in Fig. 2 (b). However, for an observer at point B' in Fig. 2 (b) the screw configuration is identical to the configuration for the observer at point B in Fig. 2(a). Because of the time-independent nature of the flow in the moving reference frame, the velocity at point A' in the screw configuration at $t + \Delta t$ is the same as velocity at point A'' in the screw configuration at time t, where the distance $A'A''$ is $-V_{ref}\Delta t$. However, it should be noted that three-dimensional simulation of the flow is performed only in a portion of the extruder. In the current work, the simulation was performed for extruder length of one and a half times the screw lead. With the flow simulated in only a portion of the screw extruder, point A'' may lie outside the domain used for flow simulation. However, the periodic nature of the flow domain in a screw extruder can be exploited to determined the velocity beyond the domain used for flow simulation. For an isothermal flow in a screw extruder, the velocity at a point is identical to

that of points which are at axial distance of nL from the point, where L is screw lead and n is an integer. In the present work, point A'' was mapped to middle one-lead length of the flow domain and the scheme described above was used to trace the particles up to a distance of 90 mm from the entrance, even though the flow domain used for simulation is only 45 mm long.

Flow Simulation in a Twin-Screw Extruder

In the present work, PELDOM™ software [9] was used to simulate the flow in co-rotating twin-screw extruder. The geometry of twin-screw extruder used for the flow simulation is the same as that of the extruder used by Shah and Gupta [10]. Fig. 3 shows the finite element mesh used for the flow simulation. For the flow simulation, the screws were rotated at 60 RPM. Since the present work at this point is not focused on predicting the quality of mixing for a specific polymer, for the time being, a Newtonian fluid with a constant viscosity of 1160 Pa·s was used in the simulation and the non-isothermal effects were ignored.

Fig. 4 shows the predicted velocity distribution at a cross-section of the twin-screw extruder. Arrows in Fig. 4 show the direction of velocity vector, whereas the magnitude is depicted by the color of the arrow. In the co-rotating extruder, velocity is the maximum at the tip of the screw flight. One important characteristic of the velocity distribution in a co-rotating twin-screw extruder is that in one screw rotation most fluid in one lobe is transferred to the other. Because of the swapping of polymer between the two lobes, a co-rotating twin-screw extruder is expected to provide a good mixing, which explains its popularity for applications such as compounding, mixing, devolatilization and chemical reaction.

Simulation of Distributive Mixing in a Twin-Screw Extruder

Starting with the 1000 blue and 1000 red particles segregated in the two halves of the twin-screw extruder entrance ($z = 0$), at four locations along the axial direction the particle distribution predicted using the particle tracing scheme discussed above is shown in Fig. 5. It is noted that starting with blue and red particles in the left and right lobes, respectively, at z = 30 mm the left lobe has more red particles, whereas the right lobe has more blue particles. That is, a major portion of the fluid in the two lobes at the entrance has been swapped to the other lobe by z = 30 mm. At z = 90 mm, the particles distribution in the twin-screw extruder in Fig. 5 (d) is quite uniform.

To determine the color homogeneity index (Eqn. 2), the outer bounding rectangle at each cross-section of the twin-screw extruder was divided into 100, 500 and 1000 equal size bins. It should be noted that some of these bins may not lie in the twin-screw extruder flow domain. Only the bins which partially or fully lie in the flow domain were used for color homogeneity calculations. The

predicted evolution of color homogeneity index along the screw axis is shown in Fig. 6. As expected, the uniformity of particle distribution, and therefore, the color homogeneity index increases with the flow along the twin-screw extruder. Also, for the same particle distribution, the homogeneity index decreases as the number of bins is increased, which is reasonable since the color homogeneity is expected to decrease as the area of observation is refined.

Simulation of Simultaneous Distributive and Dispersive Mixing in a Twin-Screw Extruder

To study the effect of particle erosion on color homogeneity index along the extruder channel, as shown in Fig. 7 (a), 200 blue and 200 red segregated agglomerates are placed in the two halves of the twin-screw extruder entrance. Using the scheme described in section 5 these particles were traced down the twin-screw extruder channel. In reference [2], Manas-Zloczower *et al.* used 0.5 mm and 0.11 mm respectively for agglomerate and fragment radii, which results in total of 93 fragments that could be eroded from a single agglomerate. In order to reduce the number of fragments, which is required for improved computational efficiency, in the present work, agglomerate and fragment radii are preset to 0.30 and 0.10 mm, respectively. With the agglomerate and fragment radii selected here, the maximum number of fragments can be eroded from an agglomerate is only 26. In the present work, new fragments were placed at distance of R from the agglomerate center, where R is the current radius of the agglomerate. The orientation of the line connecting the centers of the agglomerate and the new fragment was determined by a random number generator. Spatial distributions of the agglomerates and eroded fragments at four different locations along the twin-screw extruder are shown in Fig. 7. With only 400 agglomerates at the entrance in Fig. 7 (a), because of the erosion of a large number of fragments from the agglomerates total number of particles has increased sharply down the channel in Fig. 7 (b) - (d). Similar to the pattern observed in Fig. 5 (b), even with dispersive mixing in Fig. 7 (b) there are more red particles in left lobe than in the right lobe.

The increase in the number of particles and corresponding reduction in the agglomerate radius, as predicted by Eqn. (4) is shown in Fig. 8. As shown in Fig. 7 (a), all red agglomerates were placed in the translational region of the right lobe entrance, whereas part of blue agglomerates was placed in the intermeshing region of the left lobe entrance. Because of the difference in the initial placement of the red and blue particles, the flow histories of the two groups of the agglomerates are different. The difference in the flow histories results in the difference in the increase in the number of the two groups of particles in Fig. 8. The increase in the number of blue particles in Fig. 8, and hence the reduction in radius of the blue particles, is larger than that for the red particles.

For mixing system with 400 red and blue particles, Fig. 9 shows the increase in the color homogeneity index as the particles are convected with the polymer. To examine the effect of particle dispersion on mixing quality, increase in color homogeneity index due to purely distributive mixing (that is, number of particles remains 400) and the increase due to combined dispersive and distributive mixing (that is, number of particles increases due to erosion) is shown separately. The difference in the two curves is due to dispersive mixing. As expected, with combined distributive and dispersive mixing the increase in the color homogeneity index is larger than the increase in the index with distributive mixing alone. It is also noted that the increase in the color homogeneity index due to distributive mixing only in Fig. 9 is smaller than that in Fig. 6. The color homogeneity index in Fig. 6 was for 2000 particles whereas the index in Fig. 9 is for 400 particles only. For the larger number of particles, as expected, the uniformity of the mixing, and hence, the color homogeneity index is larger.

Conclusions

In the present work, a moving reference frame was used to trace path lines in a co-rotating twin-screw extruder. Particle spatial distribution, as well as color homogeneity index, was predicted to evaluate the distributive and dispersive mixing in the twin-screw extruder. It was shown that the color homogeneity index due to distributive mixing increased along the flow and decreased as the number of bins was increased. Moreover, the dispersive mixing significantly increased the color homogeneity index and resulted in a better overall mixing in the twin-screw extruder.

References

1. K. Alemaskin, I. Manas-Zloczower, M. Kaufman, *SPE ANTEC Tech. Papers*, **51**, 255 (2005).

2. K. Alemaskin, I. Manas-Zloczower, M. Kaufman, *SPE ANTEC Tech. Papers*, **49**, 268 (2003).

3. C. E. Shannon, *The Bell System Technical J.*, **27**, 37 (1948).

4. A. Scurati, I. Manas-Zloczower, D. Feke, *ACS, Rubber Div. Meeting*, paper 52, GA (2002).

5. A. Scurati, D. L. Feke, I. Manas-Zloczower, *Chem. Eng. Sci.*, **60**, 6564 (2005).

6. D. G. Baird, D. I. Collias, *Polymer Processing*, John Wiley and Sons, Inc., New York (1998).

7. W. Wang, I. Manas-Zloczower, D. Feke, *SPE ANTEC Tech. Papers*, **47**, 220 (2001).

8. W. Wang, I. Manas-Zloczower, *Polym. Eng. Sci.*, **41**, 1068 (2001).

9. PELDOM software, Plastic Flow, LLC, 1206 Birch Street, Houghton, MI 49931.

10. A. Shah, M. Gupta, *SPE ANTEC Tech. Papers*, **50**, 44 (2004).
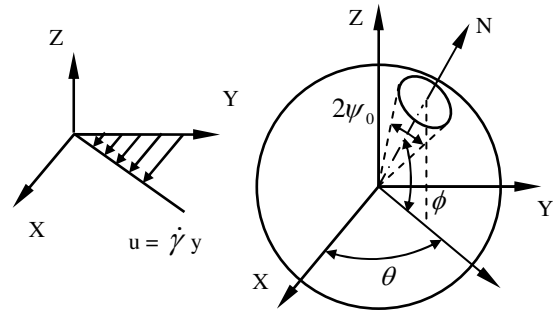
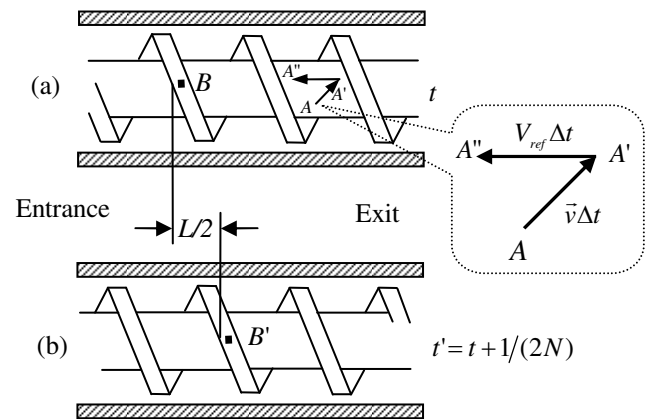Fig. 1   Schematic representation of the fragmental cap eroded off an agglomerate.

Fig. 2   Particle tracing scheme with screw rotation, (a) Screw configuration at time t, (b) Screw configuration at time $t + \Delta t$.
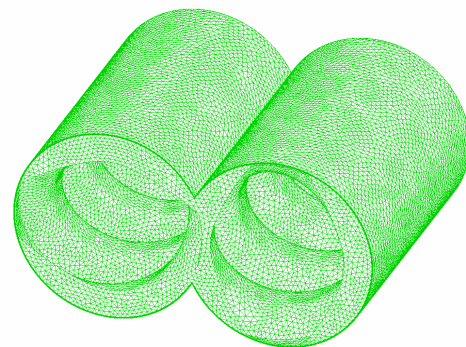

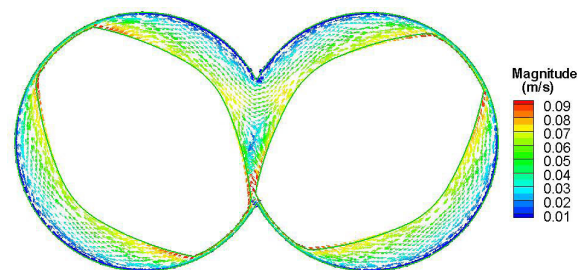Fig. 3   Finite element mesh used for flow simulation in a co-rotating twin-screw extruder.

Fig. 4   Velocity distribution in a cross-sectional plane perpendicular to the axis of twin-screw extruder (z = 11 mm).
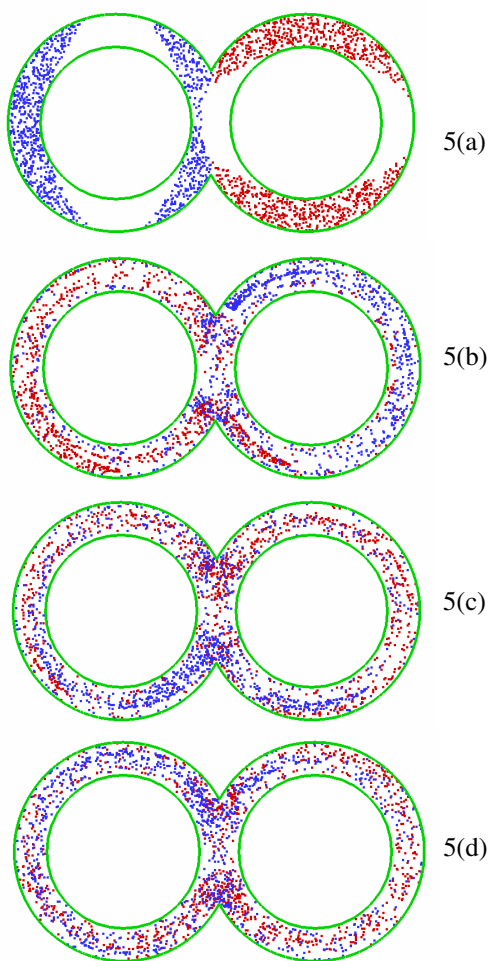
5(a)

5(b)

5(c)

5(d)

Fig. 5 Change in the spatial distribution due to distributive mixing of 2000 particles at different axial locations, z = 0 (a), 30 (b), 60 (c), 90 mm (d).
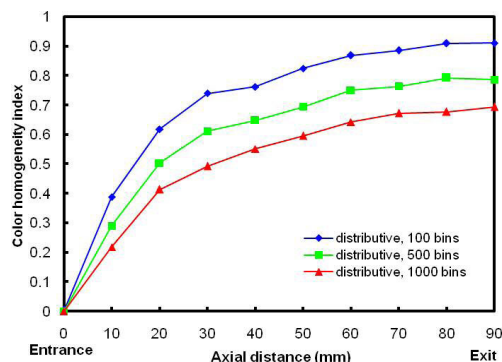

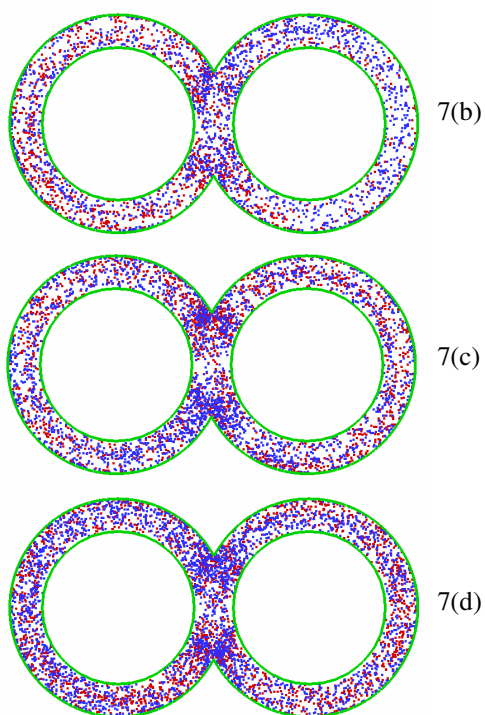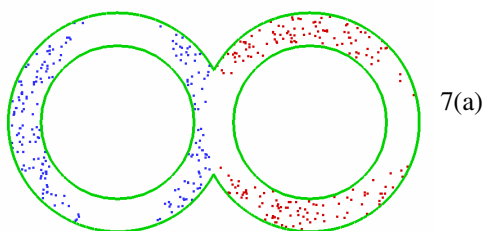Fig. 6 For 2000 particles, evolution of color homogeneity index due to distributive mixing in a twin-screw extruder.

7(a)

7(b)

7(c)

7(d)

Fig. 7 Change in spatial distribution due to combined dispersive and distributive mixing of 400 agglomerates initially placed at entrance (z = 0) cross-section, z = 0 (a), 30 (b), 60 (c), 90 mm (d).
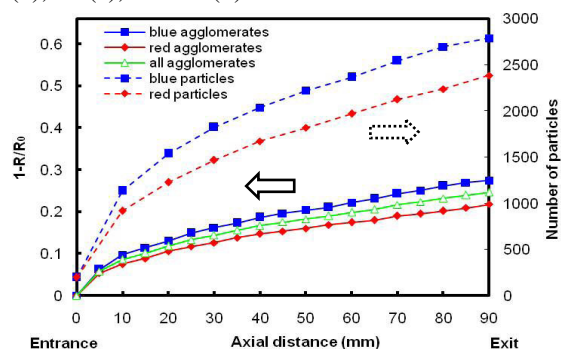

Fig. 8 Reduction of agglomerates radius and increase in the number of particles along the twin-screw extruder.
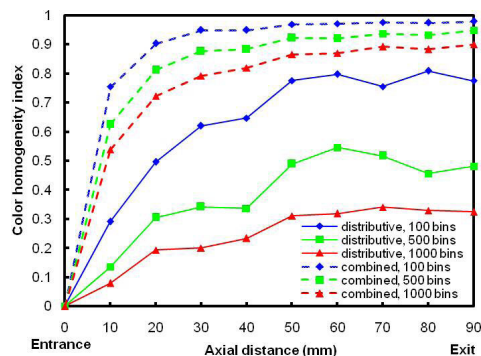

Fig. 9 Evolution of color homogeneity index for 400 agglomerates along the twin-screw extruder.